UHasselt Computational Mathematics Preprint Series

Efficient high-order discontinuous Galerkin computations of low Mach number flows

Jonas Zeifang, Klaus Kaiser, Andrea Beck, Jochen Schütz, Claus-Dieter Munz

UHasselt Computational Mathematics Preprint
Nr. UP-17-04

May 26, 2017

Efficient high-order discontinuous Galerkin computations of low Mach number flows

Jonas Zeifang[◇], Klaus Kaiser[*,†], Andrea Beck[◇], Jochen Schütz[†], Claus-Dieter Munz[◇]

May 26, 2017

In this work, we consider the efficient approximation of low-Mach flows by a high-order scheme. This scheme is a coupling of a discontinuous Galerkin (DG) discretization in space and an implicit/explicit (IMEX) discretization in time. The splitting into linear implicit and nonlinear explicit parts relies heavily on the incompressible solution. The method has been originally developed for a singularly perturbed ODE and applied to the isentropic Euler equations. Here, we improve, extend and investigate the so called RS-IMEX splitting method. The resulting scheme can cope with a broader range of Mach numbers without running into roundoff errors, it is extended to realistic physical boundary conditions and it is shown to be highly efficient in comparison to more standard solution techniques.

◇ IAG, Universität Stuttgart, Pfaffenwaldring 21,D-70569 Stuttgart
* IGPM, RWTH Aachen University, Templergraben 55, D-52062 Aachen
† Faculty of Sciences, Hasselt University, Agoralaan Gebouw D, BE-3590 Diepenbeek

Keywords: discontinuous Galerkin, IMEX-Runge-Kutta, low Mach number, splitting, asymptotic preserving

1 Introduction

Computing solutions to singularly perturbed problems can be cumbersome and expensive due to their multi-scale nature. However, they do often occur in physical reality. A typical example is the transition from the compressible to the incompressible Navier-Stokes equations that constitutes a singularly perturbed limit [27, 37, 45]. Another example are multiphase flows, in which small liquid droplets are suspended in a gaseous phase. In such problems, the Mach number ε – the local ratio of flow speed to the speed of sound – can vary by orders of magnitude. In particular, some parts are very close to the incompressible regime, meaning that the Mach number is close to zero, while in other parts, ε is of the order of one. Flows of this nature are sometimes called *all-speed* flows.

Besides some issues such as the high-order treatment of the ubiquitous shocks or the treatment of turbulence, the efficient discretization of the $\varepsilon = \mathcal{O}(1)$ case is by now rather well understood, see, e.g., [43] and the references therein. In this work, we therefore focus on the efficient discretization of the $\varepsilon \ll 1$ case as a milestone towards *all-speed* schemes.

The first idea that comes to mind is to treat the low-Mach case as incompressible. In many situations however, compressible effects matter even in the vicinity of the incompressible regime. An example is given by the computation of transcritical droplets in a surrounding (supercritical) gas phase, where a strong coupling of thermodynamics and hydrodynamics in the droplets occurs. This phase state is also called

the "compressible liquid" state and of current research interest [25, 24, 40]. Other situations occur in meteorological flows, where density gradients have to be considered but acoustic waves do not have to be resolved [13] and situations with strong temperature gradients but low velocities, e.g. natural convection [32]. As a consequence, we therefore stick to solution procedures for the compressible equations. The incompressible equations will nonetheless serve as a building block in our discretization.

Computing solutions to the low-Mach equations ($\varepsilon \ll 1$) using classical discretization paradigms which mostly rely on *explicit* time stepping methods leads to the unwanted encounter of having to choose an extremely small time step size ($\Delta t \lesssim \varepsilon \Delta x$) to obtain a stable algorithm. Furthermore, due to the excessive amount of numerical viscosity that is added to the approximate solution, the explicit method may yield an incorrect solution [35]. One remedy is to use an implicit-explicit (IMEX) time stepping method [2, 26, 9] that relies on a splitting of the flux functions into a stiff part ,which accounts for the singularity in the problem and is treated implicitly, and a non-stiff part, which only has a mild dependency on ε, and not on ε^{-1}. A number of splittings have been developed over the past few years, see, e.g., [28, 8, 12, 19]. All of those splittings have the disadvantage that it is very difficult to adapt them to other physical situations at hand, because they are developed for a specific set of equations.

To circumvent this problem, Kaiser et al. have introduced a general splitting and have applied it to the isentropic Euler equations in [23] that is based on the incompressible limit solution (being called *reference solution*), the splitting was hence termed *RS-IMEX*. The RS-IMEX idea is conceptually similar to the one introduced in [38] where the underlying problem is a singularly perturbed ODE. Related ideas have already been published earlier in [15, 8, 17]. One of the advantages of the splitting is that its idea, at least from a conceptual point of view, is independent from the underlying singularly perturbed problem and thereby not specific to a fixed system of equations. Furthermore, the implicit part is always linear in the solution variable, which usually reduces the time-to-solution tremendously, as the resulting algebraic equations are then also linear. Those linear equations are usually solved through a Krylov-type iteration method, which means that only matrix-vector products are needed, where the Jacobian is being frequently approximated via finite differences. For a nonlinear operator at low ε, this can pose severe problems for the approximation quality. However, as the implicit part of the RS-IMEX is linear, the finite differences are no approximations but exact. In [22], the splitting has been used within a high-order IMEX discontinuous Galerkin (DG) solver and it has been shown that the algorithm preserves the asymptotics of the problem, which means that for $\varepsilon \to 0$, the discrete solution converges towards a discretization of the incompressible Euler equations. The latter is an important property as it means that no spurious effects stemming from the discretization and polluting the solution are introduced for small Mach numbers.

The purpose of this work is to improve, extend and investigate the method introduced in [22] towards engineering problems:

- We improve the scheme for very small Mach numbers to suffer less from roundoff errors [30]. This is achieved through a reformulation of the method in a perturbed variable, partly following the lines of [39]. Thereby, we alleviate the dependency of the method on ε^{-1} to a great extend, which is the core source of roundoff problems.

- We extend the scheme to cope with more realistic physical settings by adding appropriate boundary conditions ([22] work with periodic ones) and considering three-dimensions.

- We investigate the scheme with respect to runtime in the framework of a modern parallel-architecture solver and compare it against other methods. For solving the algebraic system, we take advantage of the linearity of the RS-IMEX in the solution process. We demonstrate the advantages of this novel method with respect to runtime and accuracy as a function of ε for non-trivial test cases.

The paper is structured as follows. In Sec. 2 we introduce the underlying isentropic Euler equations. Sec. 3 introduces the RS-IMEX splitting for those equations, subsequently, in Sec. 4, the discontinuous Galerkin

discretization including the IMEX time discretization is detailed. In Sec. 5, we validate the method through a manufactured solution. Furthermore, we explain in detail how to circumvent a problem with machine accuracy due to low Mach numbers ε. In Sec. 6 we present more involved numerical examples and discussions concerning accuracy and efficiency in the low Mach number case. Finally, in Sec. 7 we offer conclusion and outlook.

2 Equations

In this work we consider the isentropic Euler equations on a domain $\Omega \subset \mathbb{R}^d$. Non-dimensionalized, those equations are given by

$$\begin{aligned} \partial_t \boldsymbol{w} + \nabla_x \cdot \boldsymbol{F}(\boldsymbol{w}) = 0 \qquad \text{with} \qquad \boldsymbol{w} &:= \begin{pmatrix} \rho \\ \rho \boldsymbol{u} \end{pmatrix} \\ \text{and} \qquad \boldsymbol{F}(\boldsymbol{w}) &:= \begin{pmatrix} \rho \boldsymbol{u} \\ \rho \boldsymbol{u} \otimes \boldsymbol{u} + \frac{1}{\varepsilon^2} p(\rho) \cdot \mathbf{Id} \end{pmatrix}. \end{aligned} \tag{1}$$

with $\boldsymbol{u}$ and ρ denoting velocity and density, respectively. The subscripts t and x denote temporal and spatial derivatives, respectively. The reference Mach number, defined as

$$\varepsilon := \frac{u^*}{\sqrt{p(\rho^*)/\rho^*}}$$

with u^* and ρ^* reference values used in the non-dimensionalization process, is a measure for the compressibility of the system. The pressure p is defined by the equation of state

$$p(\rho) = \kappa \rho^\gamma, \tag{2}$$

with $\gamma \geq 1$ the isentropic coefficient and $\kappa > 0$ being a constant.

The eigenvalues of $\frac{\partial}{\partial \boldsymbol{w}} \boldsymbol{F}(\boldsymbol{w}) \cdot \boldsymbol{n}$ are, for $\Omega \subset \mathbb{R}^3$ and with $c := \sqrt{\frac{\gamma p}{\rho}}$ being the speed of sound, given by

$$\lambda_{1,2} = \boldsymbol{u} \cdot \boldsymbol{n}, \qquad \lambda_{3,4} = \boldsymbol{u} \cdot \boldsymbol{n} \pm \frac{c}{\varepsilon}. \tag{3}$$

It is obvious that for $\varepsilon \ll 1$ (the low Mach case) those waves have extremely different speeds, i.e. wave speeds are in $\mathcal{O}(1)$ and $\mathcal{O}(\varepsilon^{-1})$. In the limit $\varepsilon \to 0$ two wave-speeds tend to infinity meaning that the associated hyperbolic equation degenerates. This means that some information travels infinitely fast, and some at finite speed. Besides that, one can show that under certain conditions [27], the compressible equations (1) transform towards the incompressible Euler equations, which are given by

$$\begin{aligned} \partial_t \begin{pmatrix} 0 & \\ & \mathbf{1} \end{pmatrix} \boldsymbol{w}_{(0)} + \nabla_x \cdot \boldsymbol{G}(\boldsymbol{w}_{(0)}, p_{(2)}) = 0 \qquad \text{and} \qquad \rho_{(0)} \equiv \text{const}, \\ \text{with} \qquad \boldsymbol{w}_{(0)} := \begin{pmatrix} \rho_{(0)} \\ (\rho \boldsymbol{u})_{(0)} \end{pmatrix} \\ \text{and} \qquad \boldsymbol{G}(\boldsymbol{w}_{(0)}, p_{(2)}) := \begin{pmatrix} (\rho \boldsymbol{u})_{(0)} \\ \frac{(\rho \boldsymbol{u})_{(0)} \otimes (\rho \boldsymbol{u})_{(0)}}{\rho_{(0)}} + p_{(2)} \cdot \mathbf{Id} \end{pmatrix}. \end{aligned} \tag{4}$$

The relation between the compressible and the incompressible equations can be understood best if we assume that every quantity of Eqn. (1) can be represented by an asymptotic expansion, e.g.,

$$\rho = \rho_{(0)} + \varepsilon \rho_{(1)} + \varepsilon^2 \rho_{(2)} + \mathcal{O}(\varepsilon^3),$$

and compute the formal limit $\varepsilon \to 0$. The incompressible equations (4) are then obtained under the assumption of *well-prepared* initial and boundary conditions, see e.g., [19] for a detailed computation and [27] for a more formal proof.

Definition 1 (Well-prepared initial and boundary conditions)**.** *We call initial conditions* well-prepared *if they possess an asymptotic expansion in positive powers of ε, and*

$$\rho(t=0) = const + \mathcal{O}(\varepsilon^2) \qquad and \qquad \nabla_x \cdot (\rho \boldsymbol{u})(t=0) = \mathcal{O}(\varepsilon).$$

We call boundary conditions well-prepared *if they ensure*

$$\int_{\partial\Omega} (\rho \boldsymbol{u})|_{\partial\Omega} \cdot \boldsymbol{n} = 0 \qquad and \qquad \rho|_{\partial\Omega} = const + \mathcal{O}(\varepsilon^2).$$

For *well-prepared* initial conditions the corresponding incompressible state can be calculated by setting $\varepsilon = 0$. Consequently, incompressible density is the constant value $\rho_{(0)}$ and the velocity field is $\boldsymbol{u}_{(0)}$. To initialize $p_{(2)}$ we compute

$$p = p(\rho_{(0)}) + p'(\rho_{(0)})\varepsilon^2\rho_{(2)} + \mathcal{O}(\varepsilon^4) = p_{(0)} + \varepsilon^2 p_{(2)} + \mathcal{O}(\varepsilon^4).$$

After reformulation one obtains

$$p_{(2)} = p'(\rho_{(0)})\rho_{(2)} = \kappa\gamma(\rho_{(0)})^{\gamma-1}\rho_{(2)} = \frac{1}{\varepsilon^2}\kappa\gamma(\rho_{(0)})^{\gamma-1}(\rho - \rho_{(0)}). \tag{5}$$

3 RS-IMEX

In this section, we explain the basic ideas of the RS-IMEX splitting of the isentropic Euler equations for nearly incompressible flows, more details of the final algorithm are given in Sec. 4. Previously in Sec. 2, we have seen that the isentropic Euler equations (1) in the low Mach regime transform to the incompressible Euler equations (4) if $\varepsilon \to 0$. A proper numerical method should be designed in such a way that it can imitate this behavior, i.e. for $\varepsilon \to 0$ the method should formally transform into a discretization of the incompressible equations. This is the so-called *asymptotic preserving* property, see e.g. [21].

One way to handle this type of equations is to split the flux function $\boldsymbol{F}$ into two parts and treat one part $\widehat{\boldsymbol{F}}$ with an explicit and the other part $\widetilde{\boldsymbol{F}}$ with an implicit method,

$$\partial_t \boldsymbol{w} + \nabla_x \cdot \left(\widetilde{\boldsymbol{F}}(\boldsymbol{w}) + \widehat{\boldsymbol{F}}(\boldsymbol{w})\right) = 0. \tag{6}$$

This technique results in IMEX time integration schemes, see e.g. [2, 26] and Sec. 4. For stability, efficiency and accuracy it is important to find a suitable splitting. One splitting developed in the past years is the so-called RS-IMEX, where RS stands for *reference solution*. This splitting fulfills the asymptotic preserving property in the setting of low and high-order discretizations for the isentropic Euler equations [23, 22]. Furthermore, it gave promising results for different types of equations in the sense of stability [22, 46], efficiency [23] and accuracy [23, 22].

Definition 2 (RS-IMEX splitting)**.** *The RS-IMEX splitting is defined by*

$$\widetilde{\boldsymbol{F}}(\boldsymbol{w}) = \boldsymbol{F}(\boldsymbol{w}_{(0)}) + \boldsymbol{F}'(\boldsymbol{w}_{(0)})(\boldsymbol{w} - \boldsymbol{w}_{(0)}) \qquad and \qquad \widehat{\boldsymbol{F}} = \boldsymbol{F}(\boldsymbol{w}) - \widetilde{\boldsymbol{F}}(\boldsymbol{w})$$

for a given reference solution $\boldsymbol{w}_{(0)}$ and $\boldsymbol{F}'(\boldsymbol{w}_{(0)})$ being the Jacobian of the flux

$$\boldsymbol{F}'(\boldsymbol{w}_{(0)}) = \frac{\partial \boldsymbol{F}(\boldsymbol{w}_{(0)})}{\partial \boldsymbol{w}_{(0)}}.$$

In general one could choose an arbitrary reference solution, but in the following we use the limit $\boldsymbol{w}_{(0)} = \lim_{\varepsilon \to 0} \boldsymbol{w}$, which corresponds to the solution of the incompressible equation. Applying the splitting to the isentropic Euler equations gives the following implicit and explicit parts

$$\widetilde{\boldsymbol{F}} = \begin{pmatrix} \rho \boldsymbol{u} \\ -\rho \boldsymbol{u}_{(0)} \otimes \boldsymbol{u}_{(0)} + \rho \boldsymbol{u} \otimes \boldsymbol{u}_{(0)} + \rho \boldsymbol{u}_{(0)} \otimes \boldsymbol{u} + \frac{(p(\rho_{(0)}) + p'(\rho_{(0)})(\rho - \rho_{(0)})}{\varepsilon^2} \cdot \mathbf{Id} \end{pmatrix}$$

$$\widehat{\boldsymbol{F}} = \begin{pmatrix} 0 \\ \rho(\boldsymbol{u} - \boldsymbol{u}_{(0)}) \otimes (\boldsymbol{u} - \boldsymbol{u}_{(0)}) + \frac{p(\rho) - p(\rho_{(0)}) - p'(\rho_{(0)})(\rho - \rho_{(0)})}{\varepsilon^2} \cdot \mathbf{Id} \end{pmatrix}$$

Considering the $\mathcal{O}(\varepsilon^{-2})$ terms, one obtains one motivation for the chosen reference solution. Since $\rho - \rho_{(0)} = \mathcal{O}(\varepsilon)$ one obtains

$$p(\rho) - p(\rho_{(0)}) - p'(\rho_{(0)})(\rho - \rho_{(0)}) = \mathcal{O}(\varepsilon^2).$$

So, upon inserting the exact solution, there are no stiff terms remaining in the explicit part. Of course this is only a rational that stands behind the scheme. Computing the eigenvalues of the non-stiff part explicitly, one obtains

$$\widehat{\lambda}_{1,2} = \left(\boldsymbol{u} - \boldsymbol{u}_{(0)}\right) \cdot \boldsymbol{n}, \qquad \widehat{\lambda}_3 = 0 \qquad \text{and} \qquad \widehat{\lambda}_4 = 2\left(\boldsymbol{u} - \boldsymbol{u}_{(0)}\right) \cdot \boldsymbol{n},$$

and indeed, these eigenvalues are $\mathcal{O}(1)$. Even more, upon inserting the exact solution, they would be in $\mathcal{O}(\varepsilon)$ for this given choice of the reference solution. Fast waves are solely solved with the implicit method, which is a core requirement for unconditional stability with respect to ε.

Remark 1. *A similar technique has been used for the stiff collision operator of kinetic equations in [15] and for the pressure gradient of shallow-water equations in [8, 18].*

4 Discretization

4.1 High Order Discontinuous Galerkin IMEX Framework

Discontinuous Galerkin (DG) schemes have recently gained considerable interest as baseline schemes for multiscale problems, see, e.g., [5, 3, 10, 43] and the references therein. They can be interpreted as a hybrid finite element - finite volume formulation, where an element-wise Galerkin variational formulation is coupled weakly to its neighbors through a numerical flux term. Each inner-element solution is approximated by a polynomial function of given order $\mathcal{N}$. Penalization of discontinuities and the locality of the basis make DG suitable for hyperbolic problems. In addition, the compact operator with small memory and communication footprint leads to excellent parallel scaling properties and the element-based approximation enables unstructured meshing of complex domains.

To obtain a DG discretization, we assume that the domain is separated into a finite number of independent cells. Then we seek a piece-wise smooth function $\boldsymbol{w_h}$, i.e. it is a polynomial of maximal degree $\mathcal{N}$ on every cell, which fulfills the weak discontinuous Galerkin formulation, given by

$$\frac{\partial}{\partial t} \int_E \boldsymbol{w_h}\, \phi(\boldsymbol{x})\, d\boldsymbol{x} + \oint_{\partial E} \boldsymbol{F}_n^* \phi(\boldsymbol{x})\, ds - \int_E \boldsymbol{F}(\boldsymbol{w_h}) \cdot \boldsymbol{\nabla}_x\, \phi(\boldsymbol{x})\, d\boldsymbol{x} = 0, \tag{7}$$

on every cell E for every polynomial test-function $\phi(\boldsymbol{x})$ of maximal degree $\mathcal{N}$. Note that $\boldsymbol{F}_n^*$ denotes the surface normal numerical flux function, given by $\boldsymbol{F}_n^* := \boldsymbol{F}_n^*(\boldsymbol{w_h}^+, \boldsymbol{w_h}^-)$ and superscripts $\pm$ denote the values at the grid cell interface from the neighbor and the local grid cell E, respectively.

The current investigations are based on a particularly efficient variant of the general DG formulation (7), namely the Discontinuous Galerkin Spectral Element method (DGSEM) proposed by [29]. In this formulation, the solution $\boldsymbol{w}$ is approximated as a tensor-product of one-dimensional Lagrange interpolating polynomials of degree $\mathcal{N}$. The $\mathcal{N}+1$ Legendre-Gauss quadrature points $\{\xi_i\}_{i=0}^{\mathcal{N}}$ are chosen as interpolation nodes. This collocation of interpolation and integration nodes significantly reduces the number of operations per degree of freedom. In particular, the tensor-product structure of the solution ansatz transfers to the operator itself, avoiding element-global volume operations. Instead, the multi-d operator is constructed of consecutive 1d-operations. One disadvantage is that this reduces the flexibility of DG with respect to meshing, as only quadrilateral meshes can be used in order not to destroy the tensor product structure.

Details on the implementation and efficiency of the solver are given by Hindenlang et al. [20]. Extension of the framework to include multiphase flow based on a sharp interface approach, large eddy simulation methods and shock capturing strategies are given by [14, 16, 6, 41]. The full FLEXI framework, including pre-and postprocessing tools, is available as open source software[1].

For the extension of this solver to an implicit-explicit time discretization we consider again a splitting as in Eqn. (6). (Note: With $\widetilde{\boldsymbol{F}}(\boldsymbol{w}) = \boldsymbol{F}(\boldsymbol{w})$ and $\widehat{\boldsymbol{F}}(\boldsymbol{w}) = 0$, also a fully implicit scheme falls into this framework.) IMEX schemes are defined by their Butcher tableaux featuring the coefficients $\widetilde{A}$, $\widehat{A}$, $\widetilde{c}$ and $\widehat{c}$. In semi-discrete form the implicit-explicit Runge-Kutta time discretization for the i^{th} stage and the n^{th} time step can be written as

$$\begin{aligned}\boldsymbol{w}^{n,i} - \boldsymbol{w}^n + \Delta t \Bigg(&\sum_{j=1}^{i} \widetilde{A}_{i,j} \nabla_x \cdot \widetilde{\boldsymbol{F}}(\boldsymbol{w}^{n,j}, t^n + \widetilde{c}_j \Delta t) \\ &+ \sum_{j=1}^{i-1} \widehat{\boldsymbol{A}}_{i,j} \nabla_x \cdot \widehat{\boldsymbol{F}}(\boldsymbol{w}^{n,j}, t^n + \widehat{c}_j \Delta t) \Bigg) = 0.\end{aligned} \tag{8}$$

A reformulation of Eqn. (8) yields

$$\begin{aligned}&\boldsymbol{w}^{n,i} + \Delta t \widetilde{A}_{i,i} \nabla_x \cdot \widetilde{\boldsymbol{F}}(\boldsymbol{w}^{n,i}, t^n + \widetilde{c}_i \Delta t) = \\ &\quad \boldsymbol{w}^n - \Delta t \sum_{j=1}^{i-1} \left[\widetilde{A}_{i,j} \nabla_x \cdot \widetilde{\boldsymbol{F}}(\boldsymbol{w}^{n,j}, t^n + \widetilde{c}_j \Delta t) + \widehat{A}_{i,j} \nabla_x \cdot \widehat{\boldsymbol{F}}(\boldsymbol{w}^{n,j}, t^n + \widehat{c}_j \Delta t) \right],\end{aligned}$$

where the right hand side is either known from previous stages or can be computed explicitly. In the following, this equation is abbreviated by

$$(\mathbf{Id} - \Delta t \widetilde{A}_{i,i} \widetilde{\boldsymbol{R}}) \boldsymbol{w}^{n,i} = \boldsymbol{b},$$

with $\widetilde{\boldsymbol{R}}$ denoting the spatial operator with the implicitly treated fluxes. To solve this potentially non-linear (for a fully implicit scheme it is, for the RS-IMEX it is linear!) system, a standard root finding algorithm such as Newton's method can be applied. Therefore, the IMEX-Runge-Kutta scheme for the k^{th} Newton's iteration reads

$$\begin{aligned}\boldsymbol{w}^{(k+1)} &= \boldsymbol{w}^{(k)} + \Delta \boldsymbol{w} \\ \Delta \boldsymbol{w} - \Delta t \widetilde{A}_{i,i} \frac{\partial \widetilde{\boldsymbol{R}}(\boldsymbol{w}^{(k)})}{\partial \boldsymbol{w}} \Delta \boldsymbol{w} &= -\boldsymbol{w}^{(k)} + \Delta t \widetilde{A}_{i,i} \widetilde{\boldsymbol{R}}(\boldsymbol{w}^{(k)}) + b.\end{aligned} \tag{9}$$

For the ease of presentation, we have omitted the superscript n, i.

[1] www.flexi-project.org, GNU GPL v3.0

Eqn. (9) is a linear system for every Newton's iteration k, which can be solved with a standard linear solving algorithm. To minimize computational costs for calculating and storing the Jacobian, the matrix free GMRES linear solving algorithm by Saad and Schultz [36] is applied and the Jacobian in Eqn. (9) is approximated via a finite difference

$$\frac{\partial \widetilde{\boldsymbol{R}}(\boldsymbol{w}^{(k)})}{\partial \boldsymbol{w}} \approx \frac{\widetilde{\boldsymbol{R}}(\boldsymbol{w}^{(k)} + \Delta_{FD}\Delta\boldsymbol{w}) - \widetilde{\boldsymbol{R}}(\boldsymbol{w}^{(k)})}{\Delta_{FD}} \tag{10}$$

for a small Δ_{FD} which can be calculated according to Quin et al. [34] as

$$\Delta_{FD} = \frac{\sqrt{eps}}{||\Delta\boldsymbol{w}||_2},$$

with *eps* being the machine accuracy. As the implicit flux of the RS-IMEX splitting is linear, this finite difference can be simplified but special care has to be taken of Dirichlet type boundary conditions. Hence, for the RS-IMEX splitting, the Jacobian can be simplified to

$$\frac{\partial \widetilde{\boldsymbol{R}}(\boldsymbol{w}^{(k)})}{\partial \boldsymbol{w}} = \widetilde{\boldsymbol{R}}(\Delta\boldsymbol{w}) - \widetilde{\boldsymbol{R}}(\boldsymbol{0}). \tag{11}$$

In our implementation, we use a standard block-Jacobian preconditioner due to the small building and storing costs of the preconditioner. This turned out to be beneficial for a DG setup with a very large number of processors [7].

4.2 Incompressible Solver

The RS-IMEX splitting, defined in Def. 2 requires the corresponding incompressible state. Therefore, an incompressible solver in the discontinuous Galerkin framework is needed. We start with the incompressible Euler equations as given in Eqn. (4) in three dimensions and reformulate them as

$$\partial_t \begin{pmatrix} 0 & \\ & \mathbf{1} \end{pmatrix} \boldsymbol{U} + \nabla_x \cdot \widetilde{\boldsymbol{G}}(\boldsymbol{U}) = 0,$$

for the state vector $\boldsymbol{U} = (p_{(2)}, u_{(0),1}, u_{(0),2}, u_{(0),3})^T$ and with the flux

$$\widetilde{\boldsymbol{G}}(\boldsymbol{U}) := \begin{pmatrix} \boldsymbol{u}_{(0)} \\ \boldsymbol{u}_{(0)} \otimes \boldsymbol{u}_{(0)} + \frac{p_{(2)}}{\rho_{(0)}} \cdot \mathbf{Id} \end{pmatrix}.$$

Note as a reminder that $p_{(2)}$ denotes the hydrodynamic pressure, $\rho_{(0)}$ is a constant positive value and $\boldsymbol{u}_{(0)} = (u_{(0),1}, u_{(0),2}, u_{(0),3})^T$ denotes the three dimensional velocity vector. As the divergence free condition for the velocity field is not a time evolution equation for the hydrodynamic pressure, a numerical flux function is required to couple the velocity and pressure field. A flux which satisfies this condition for solving incompressible flows with a discontinuous Galerkin scheme has been proposed by Bassi et al. [4]. In order to obtain a flux at the interfaces, artificial compressibility is added for the solution of the Riemann problem. An iterative Godunov-type Riemann solver is used in [4] to obtain the interface fluxes. As the accuracy of the incompressible reference solution for the RS-IMEX splitting is not crucial, we use a cheaper Lax-Friedrichs type Riemann solver motivated by the asymptotic analysis which reads

$$\widetilde{\boldsymbol{G}}^* = \frac{1}{2}\left(\widetilde{\boldsymbol{G}}(\boldsymbol{U}^+) + \widetilde{\boldsymbol{G}}(\boldsymbol{U}^-) + \mathbf{Diag}\left(\frac{{\rho_{(0)}}^{1-\gamma}}{\kappa\gamma}, 1, 1, 1\right)(\boldsymbol{U}^+ - \boldsymbol{U}^-)\right),$$

with κ and γ from the equation of state (2).

5 Validation and reformulation

In this section, we validate the code and give first impressions of its performance. Furthermore, we indicate how to avoid problems with machine accuracy when ε is very small. As an underlying example, we use the two dimensional smooth traveling vortex presented in [22]. For both compressible and incompressible isentropic Euler equations, the solution is a mere transport of an initial vortex in the x_1-direction with speed 0.5. The compressible solution reads

$$\rho(\boldsymbol{x},t) = \rho\left(\begin{pmatrix} x_1 - 0.5t \\ x_2 \end{pmatrix}, 0\right), \qquad \boldsymbol{u}(\boldsymbol{x},t) = \boldsymbol{u}\left(\begin{pmatrix} x_1 - 0.5t \\ x_2 \end{pmatrix}, 0\right),$$

for the initial conditions

$$\begin{aligned} \rho(\boldsymbol{x}, t=0) &= 2 + (500\epsilon)^2 \cdot \begin{cases} 0.5 e^{\frac{2}{\Delta r}} \Delta r - \mathrm{Ei}(\frac{2}{\Delta r}) & \text{for } r < 0.5 \\ 0 & \text{otherwise} \end{cases} \\ \boldsymbol{u}(\boldsymbol{x}, t=0) &= \begin{pmatrix} 0.5 \\ 0 \end{pmatrix} + 500 \begin{pmatrix} -x_2 + 0.5 \\ x_1 - 0.5 \end{pmatrix} \cdot \begin{cases} e^{\frac{1}{\Delta r}} & \text{for } r < 0.5 \\ 0 & \text{otherwise} \end{cases} \end{aligned} \tag{12}$$

with $r := \sqrt{(x_1 - 0.5)^2 + (x_2 - 0.5)^2}$, $\Delta r := r^2 - 0.25$ and the equation of state $p(\rho) = \kappa \rho^\gamma$ with $\kappa = 0.5$ and $\gamma = 2$. Ei denotes the exponential integral function

$$\mathrm{Ei}(x) := \int_{-\infty}^{x} \frac{e^t}{t} \mathrm{d}t.$$

In our implementation we use the algorithm by Press et al. [33] for the exponential integral function. Boundary conditions of the domain $\Omega = [0,1]^2$ are chosen to be periodic. The initialization of the incompressible pressure is obtained via Eqn. (5).

5.1 Validation

Here, we present numerical results validating the solver. As time integrators, we use the IMEX Runge-Kutta schemes IMEX-ARS-222 and IMEX-ARS-443 by [2] as 2^{nd} and 3^{rd} order schemes and IMEX-ARK-4A2 from [31] as 4^{th} order scheme. All schemes are given with their Butcher tableau in the appendix, see Tbl. 1, 2 and 3. In the numerical results, an appropriate polynomial degree is chosen so that the overall order is the order of the time integration scheme.

Fig. 1 shows the convergence of the overall L_2-error (top) for the incompressible solver and the RS-IMEX splitting. Both, the incompressible solver itself and the RS-IMEX splitting which uses the incompressible solver show the correct order of convergence. Only the 3^{rd} order case shows an order that is slightly too low, but this is inherent to the test case and has already been observed in [22] for under-resolved explicit calculations. Additionally, Fig. 1 shows the convergence in density for the RS-IMEX splitting (bottom). Here, the correct order is obtained from 2^{nd} to 4^{th} order and in contrary to the overall L_2-error, the L_2-error in density scales with ε^2. This is due to the structure of the test case and the asymptotic preserving property of the method: The density can be expressed as $\rho = \text{const} + \mathcal{O}(\varepsilon^2)$ which is a disturbance in ε^2 added to a constant – this can be reproduced exactly by the DG scheme due to the AP property. Momentum can be expressed as $\rho\boldsymbol{u} = \mathcal{O}(1)$ and therefore, the error does not scale with ε.

5.2 Efficiency

In this subsection, we evaluate the efficiency of the RS-IMEX splitting in the low Mach number limit. A desirable method has the following properties:

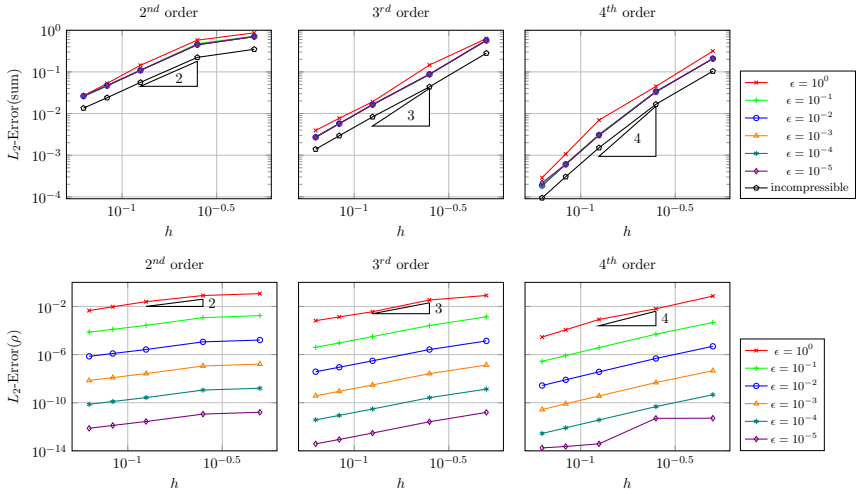

Figure 1: h-convergence of 2^{nd}, 3^{rd} and 4^{th} order incompressible and RS-IMEX scheme for traveling vortex in overall L_2-error (top) and L_2-error in density (bottom) for different Mach number.

- It is computationally cheaper than a fully implicit scheme. We have hope that this will be the case due to the linearity of the implicit flux $\widetilde{F}$.
- The scheme should - for small Mach numbers - be more efficient than a fully explicit scheme. This can also be expected, because the RS-IMEX scheme should be stable under a time step restriction that depends solely on Δx, and not on ε. An explicit scheme will always have a time step restriction of form $\Delta t \lesssim \varepsilon \Delta x$ due to the CFL condition.

For relatively large Mach numbers, we expect the RS-IMEX splitting scheme to be computationally more expensive as additional equations have to be solved. The task of this section is to identify the 'sweet spot' between an explicit and the RS-IMEX scheme.

We compare the computational effort for a fully implicit, a fully explicit and the RS-IMEX scheme in Fig. 2. The results have been obtained on 16 cores with a temporal and spatial order of four. As time integration scheme we used the IMEX-ARK-4A2 [31] for RS-IMEX, the implicit part of the same scheme for the implicit method and a five-stage Runge-Kutta scheme [11] (see Tbl. 5) for the explicit part. For all computations we start with the same grid and perform several refinements.

CFL numbers were chosen as $CFL = 0.9$ for the explicit scheme, $CFL = 150$ for the implicit scheme and $CFL = 0.5$ for the RS-IMEX scheme. For the fully implicit and explicit scheme, the CFL condition is calculated using the eigenvalues of the unsplit system (3), whereas the RS-IMEX splitting only uses the convective eigenvalue ($\lambda_{1,2}$ in (3)). Our computations showed that for the implicit scheme $CFL = 150$ is a good compromise between required time steps and required iterations per time step. (Note that the performance of a *linear* solver depends heavily on Δt, Δx and ε.)

First of all, we can conclude from Fig. 2 that RS-IMEX computes a smaller error on the same grid compared to the other methods (the i^{th} dot of each graph corresponds to the same grid).

It can be seen from Fig. 2 that the computational time of the explicit and the implicit scheme scales somehow inversely to the Mach number. Since the equation-system gets more and more stiff for $\varepsilon \ll 1$ the computational cost of the implicit method grows faster than the explicit ones. For the RS-IMEX only a slight increase in computational time is noticeable for a decreasing Mach number.

If the efficiency is defined as the quotient of error and computational effort, the efficiency of the explicit and implicit scheme decreases stronger than for the RS-IMEX splitting with decreasing ε due to the

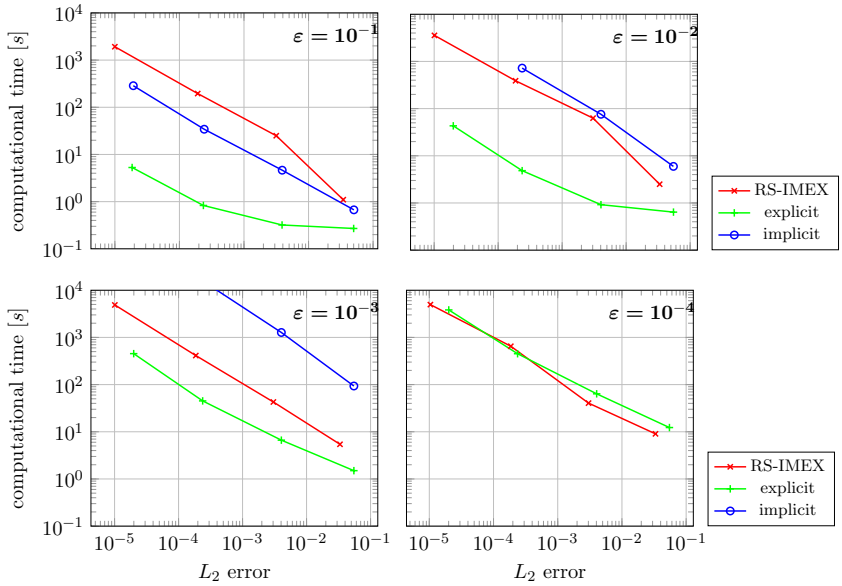

Figure 2: Comparison of computational time for 2d traveling vortex (4^{th} oder in space and time) with respect to overall L_2 error.

aforementioned scaling.

The implicit method shows an extreme growth in computational cost and therefore for $\varepsilon \leq 10^{-2}$ the efficiency of the implicit method becomes worse than the efficiency of the RS-IMEX method. The explicit method reaches this sweet spot for a much smaller value of ε, i.e. for $\varepsilon \leq 10^{-4}$ since the computational cost of the explicit method is much smaller. Note that fully implicit calculations with $\varepsilon = 10^{-4}$ are not displayed as machine accuracy issues caused by the finite difference (10) lead to an extremely strong increase in computational time due to slow convergence.

We computed the same tests for a lower spatial order (2^{nd} order in space and 4^{th} order in time) and a higher spatial order (8^{th} order in space and 4^{th} order in time) and obtained similar results with an earlier (low order case) and later (higher order case) break even point. This behavior can be explained by the worsening of an implicit high order scheme due to increasing storage requirements.

More improvements concerning efficiency are obtained if the error in density is considered, displayed in Fig. 3. Again, the i^{th} symbol of each line corresponds to the same mesh. Therefore, it is visible that for low Mach numbers one obtains significantly lower errors with the RS-IMEX scheme than with the fully explicit scheme with the same mesh. The graph shows that the RS-IMEX splitting is more efficient than the explicit scheme for Mach numbers $\varepsilon \leq 10^{-3}$. The steepening of the $\varepsilon = 10^{-4}$ RS-IMEX line is due to round off errors, which occur due to machine precision. We take a closer look on this problem in the next subsection.

5.3 Solving in the Perturbation

It has to be noted that for very small Mach numbers, the equation becomes extremely stiff and therefore limited machine accuracy can be a problem. Indeed, in [22] the authors observed problems with the accuracy for the RS-IMEX discretization for small values of ε which cannot be explained by order reduction [9]. Similar problems have been seen in Fig. 3. This observation serves as a motivation to rewrite the method similarly

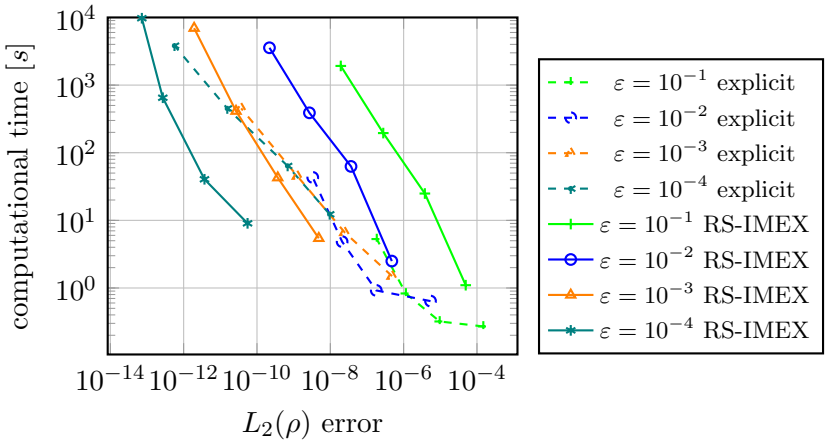

Figure 3: Comparison of computational time for 2d traveling vortex (4^{th} oder in space and time) with respect to L_2 error in density.

to the proceeding in [39]. The key trick is to rewrite the solution $\boldsymbol{w}$ as

$$\boldsymbol{w} = \underbrace{\boldsymbol{w}_{(0)}}_{\text{reference solution}} + \varepsilon \underbrace{\left(\boldsymbol{w}_{(1)} + \varepsilon \boldsymbol{w}_{(2)} + \mathcal{O}(\varepsilon^2)\right)}_{\text{perturbation}} =: \boldsymbol{w}_{(0)} + \varepsilon \delta \boldsymbol{w}$$

and to observe that $\boldsymbol{w}_{(0)}$ is already part of the algorithm and therefore known, so one only has to solve in the perturbation $\delta \boldsymbol{w}$ which fulfills the equation

$$\partial_t \boldsymbol{w}_{(0)} + \varepsilon \partial_t \delta \boldsymbol{w} + \nabla_x \cdot \left(\widetilde{\boldsymbol{F}} \left(\boldsymbol{w}_{(0)} + \varepsilon \delta \boldsymbol{w} \right) + \widehat{\boldsymbol{F}} \left(\boldsymbol{w}_{(0)} + \varepsilon \delta \boldsymbol{w} \right) \right) = 0.$$

In the setting of the isentropic Euler equations $\partial_t \boldsymbol{w}_{(0)}$ can be identified by the corresponding incompressible equations. Therefore, we can replace it by the flux function $\boldsymbol{G}(\boldsymbol{w}_{(0)}, p_{(2)})$ given in Eqn. (4). This results in

$$\partial_t \delta \boldsymbol{w} + \frac{1}{\varepsilon} \nabla_x \cdot \left(\widetilde{\boldsymbol{F}} \left(\boldsymbol{w}_{(0)} + \varepsilon \delta \boldsymbol{w} \right) - \boldsymbol{G}(\boldsymbol{w}_{(0)}, p_{(2)}) + \widehat{\boldsymbol{F}} \left(\boldsymbol{w}_{(0)} + \varepsilon \delta \boldsymbol{w} \right) \right) = 0,$$

where $\boldsymbol{G}$ is added to the stiff part of the equation, i.e. handled with an implicit method, but does not change the implicit matrix, since the values are given. Computing the eigenvalues of the explicit part and using $\delta(\rho \boldsymbol{u}) = \rho_{(0)} \delta \boldsymbol{u} + \boldsymbol{u} \delta \rho + \varepsilon \delta \rho \delta \boldsymbol{u}$ yields

$$\widehat{\lambda}_{1,2} = \varepsilon(\delta \boldsymbol{u} \cdot \boldsymbol{n}), \qquad \widehat{\lambda}_3 = 0 \qquad \text{and} \qquad \widehat{\lambda}_4 = 2\varepsilon(\delta \boldsymbol{u} \cdot \boldsymbol{n}).$$

Consequently, the explicit part has eigenvalues in $\mathcal{O}(\varepsilon)$ and the resulting method is supposed to show similar stability properties with an improved accuracy because many of the $\mathcal{O}(\varepsilon^{-1})$ terms drop out.

However, not all the terms cancel directly. One remaining term in the explicit flux is

$$\frac{1}{\varepsilon^2} \left(p(\rho_{(0)} + \varepsilon \delta \rho) - p(\rho_{(0)}) - p'(\rho_{(0)}) \varepsilon \delta \rho \right).$$

Using a Taylor expansion for p gives

$$p(\rho_{(0)} + \varepsilon \delta \rho) = p(\rho_{(0)}) + \varepsilon p'(\rho_{(0)}) \delta \rho + \varepsilon^2 p''(\rho_{(0)}) \delta \rho^2 + \mathcal{O}(\varepsilon^3 \delta \rho^3),$$

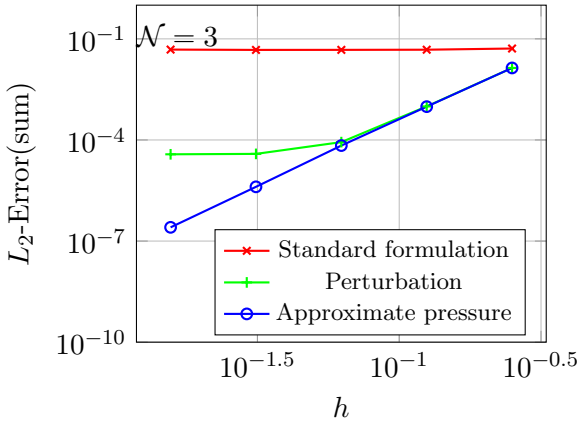

Figure 4: Convergence behavior for a 4^{th} order RS-IMEX discretization for the traveling vortex example for a very low Mach number of $\varepsilon = 10^{-6}$.

and therefore the terms read

$$\frac{1}{\varepsilon^2}\left(p(\rho_{(0)} + \varepsilon\delta\rho) - p(\rho_{(0)}) - p'(\rho_{(0)})\varepsilon\delta\rho\right) = p''(\rho_{(0)})\delta\rho^2 + \mathcal{O}(\varepsilon\delta\rho^3) \approx p''(\rho_{(0)})\delta\rho^2.$$

We can therefore substitute the expression on the left-hand side by the one on the right-hand side, we call this proceeding *approximate pressure*. Note that - in general - this introduces an additional error in $\mathcal{O}(\varepsilon\delta\rho^3)$ to the equation, but in our setting $\delta\rho = \mathcal{O}(\varepsilon)$ and therefore the error would be in $\mathcal{O}(\varepsilon^4)$. For the low-Mach case, this can safely be assume to be negligibly small. Note furthermore that for $\gamma = 2$ this does *not* introduce an additional error.

In Fig. 4 results are presented for a very small ε. Spatial and temporal accuracy is set to fourth order, i.e., we are using $\mathcal{N} = 3$ and the IMEX-ARK-4A2 scheme. We show errors for the 'straightforward' RS-IMEX discretization, for solving in the perturbation only and for solving in the perturbation with an approximated pressure. Note that for the high order vortex example the approximated pressure is an exact reformulation since $\gamma = 2$. Fig. 4 shows that due to the reformulation the problems caused by machine accuracy are tremendously reduced. All computations have been done with an exact reference solution to neglect influences due to an inaccurate incompressible solver.

6 Numerical results

In this section, we present numerical results for test cases which are more physically motivated than the one considered in the previous subsection. We start with a two-dimensional flow over a cylinder and subsequently, we investigate the three-dimensional inviscid Taylor-Green vortex.

6.1 Flow over a Cylinder

This test case demonstrates the ability to use different boundary conditions in our implementation and illustrates the importance of the *asymptotic preserving* property. We compute the two-dimensional, inviscid flow over a cylinder at low Mach numbers. We apply Euler wall boundary conditions on the surface of the cylinder and Dirichlet type boundary conditions at all other boundaries of the domain. We use a uniform two-dimensional state $\boldsymbol{w}_\infty = (\rho_\infty, u_{1,\infty}, u_{2,\infty})^T = (1.0, 1.0, 0)^T$ (in non-dimensional quantities) as initialization and for the Dirichlet boundaries. Again, the equation of state $p(\rho) = \kappa\rho^\gamma$ with $\kappa = 0.5$ and $\gamma = 2$ has been utilized. In the low Mach number limit, the exact solution is given by a potential flow

field [1]. One measure of solution quality is the pressure coefficient C_p. It can be computed in two ways, once via the equation of state

$$C_p^{\text{EOS}} = \frac{1}{\varepsilon^2} \frac{p - p_\infty}{\frac{1}{2}\rho_\infty \|\boldsymbol{u}_\infty\|_2^2} = \frac{1}{\varepsilon^2} \frac{\kappa(\rho^\gamma - \rho_\infty^\gamma)}{\frac{1}{2}\rho_\infty \|\boldsymbol{u}_\infty\|_2^2}, \tag{13}$$

and once via Bernoulli's hypothesis for an incompressible, inviscid flow [1]

$$C_p^{\text{Bernoulli}} = \frac{1}{\varepsilon^2} \frac{p - p_\infty}{\frac{1}{2}\rho_\infty \|\boldsymbol{u}_\infty\|_2^2} = 1 - \frac{\rho \|\boldsymbol{u}\|_2^2}{\rho_\infty \|\boldsymbol{u}_\infty\|_2^2}. \tag{14}$$

For an incompressible, inviscid flow the result of Eqn. (13) should coincide with the results of Eqn. (14), and therefore should hold

$$C_p^{\text{EOS}} = C_p^{\text{Bernoulli}} = 1 - 4\sin^2(\theta),$$

with θ being the angular coordinate of the cylinder's polar coordinates ranging from 0 to 2π [1]. Hence, the maximum of the pressure coefficient is $C_p = 1$ at the stagnation points and the minimum $C_p = -3$ is reached at the positions with maximum velocity on the top and bottom.

Rieper [35] showed that an explicit scheme with an HLL-type Riemann solver reproduces the wrong pressure distribution in the low Mach number limit, as it adds too much numerical viscosity. Therefore, the explicit scheme converges to creeping flow where the dynamic pressure is several orders of magnitudes too high. In contrast, an *asymptotic preserving* scheme would reproduce the potential flow correctly. This is given since we can show for a method which is asymptotic preserving that also on the discrete level

$$\rho_h = \rho_{(0)} + \mathcal{O}(\varepsilon^2)$$

holds. Note that in this case $\rho_{(0)} = \rho_\infty$. Therefore using a Taylor expansion in equation (13) we obtain

$$C_p^{\text{EOS}} = \frac{1}{\varepsilon^2} \frac{\kappa \mathcal{O}(\varepsilon^2)}{\frac{1}{2}\rho_\infty \|\boldsymbol{u}_\infty\|_2^2} = \mathcal{O}(1).$$

If the method is not asymptotic preserving, the difference in the pressure might be in $\mathcal{O}(\varepsilon)$ or worse, and therefore the pressure coefficient C_p^{EOS} becomes $\mathcal{O}(\varepsilon^{-1})$ or worse. This only affects the pressure coefficient computed via the equation of state, which is therefore an important measure of asymptotic quality of the method.

Fig. 5 shows the results of a calculation with 1,646 elements and a polynomial degree of $\mathcal{N} = 2$ using an explicit Lax-Friedrichs Riemann solver on the one hand and the RS-IMEX splitting on the other. The Mach number is set to $\varepsilon = 10^{-5}$. If the pressure coefficient is evaluated via Eqn. (14), meaning it is mainly influenced by the velocity distribution (upper row in Fig. 5), both schemes are able to predict potential flow. A different behavior is observed if the dynamic pressure is evaluated via the equation of state (lower row). Whereas the explicit scheme shows the flow pattern of a creeping flow and a pressure coefficient several orders of magnitude too high, the RS-IMEX scheme is able to reproduce the potential flow. This illustrates the *asymptotic preserving* property of the scheme. A further validation of the RS-IMEX splitting can be seen in Fig. 6 where the C_p distribution on the upper surface of the cylinder evaluated with the equation of state and with Bernoulli's hypothesis is compared with the solution for potential flow.

6.2 Taylor-Green Vortex

The Taylor-Green vortex introduced in [42] is originally a three-dimensional, incompressible viscous test case to study the transition to turbulence and its decay. For non-viscous equation systems such as the isentropic

Euler equations it can be used to investigate the amount of dissipation added by a numerical scheme. The standard incompressible initial conditions are given by

$$\begin{aligned}
\rho_{(0)} &= 1 \\
\boldsymbol{u}_{(0)}(\boldsymbol{x}, t=0) &= V_0 \begin{pmatrix} \cos(x_1)\cos(x_2)\cos(x_3) \\ -\cos(x_1)\sin(x_2)\cos(x_3) \\ 0 \end{pmatrix} \\
p_{(2)}(\boldsymbol{x}, t=0) &= \frac{\rho_{(0)} V_0^2}{16}(\cos(2x_1)+\cos(2x_2))(\cos(2x_3)+2),
\end{aligned}$$

where V_0 denotes a constant initial velocity which is chosen to be $V_0 = 1$; x_1, x_2 and x_3 denote the spatial coordinates of the periodic box $\Omega = [0, 2\pi]^3$. We adapt the initialization for the compressible isentropic Euler equations according to Eqn. (5) to obtain a consistent initial dataset for the incompressible initialization

$$\begin{aligned}
\rho(\boldsymbol{x}, t=0) &= \rho_{(0)} + \varepsilon^2 \frac{V_0^2 {\rho_{(0)}}^{2-\gamma}}{16\gamma\kappa}\left(\cos(2x_1)+\cos(2x_2)\right)\left(\cos(2x_3)+2\right), \\
\boldsymbol{u}(\boldsymbol{x}, t=0) &= V_0 \begin{pmatrix} \cos(x_1)\cos(x_2)\cos(x_3) \\ -\cos(x_1)\sin(x_2)\cos(x_3) \\ 0 \end{pmatrix},
\end{aligned}$$

with $p = \kappa\rho^\gamma$, $\kappa = 0.5$ and $\gamma = 2$. All calculations were conducted on a regular grid with 16^3 elements and a polynomial degree of $\mathcal{N} = 3$. For the temporal discretization, the third order IMEX-ARS-443 scheme by Ascher et al. [2] is used. Again, a fully implicit method is obtained if only the implicit Butcher table is considered. The explicit calculations were made with a standard three stage third order Runge-Kutta scheme [44] (see Tbl. 4). We consider the isosurfaces of the velocity field to compare the results of the RS-IMEX splitting with the explicit scheme in a qualitative manner. Fig. 7 exemplary shows the velocity field at a Mach number of $\varepsilon = 10^{-4}$ for two different times t. In the top row, the solutions of both the explicit and the RS-IMEX scheme are identical. For consistent schemes, this is to be expected, since at this early (pre-transition) state, the chosen discretization is sufficient to completely resolve the occurring scales. This notion is also supported in Fig 8, where the kinetic energy, defined as

$$E_{kin,comp} = \frac{\varepsilon^2}{2}\rho\|\boldsymbol{u}\|_2^2,$$

is preserved at $t = 3s$ for both schemes. The kinetic energy can be used as a benchmark of numerical dissipation properties of a scheme for inviscid flows. In the bottom row of Fig. 7, the solutions for $t = 7s$ are shown. Here, clear qualitative differences exist and the kinetic energy is no longer conserved, which can be attributed to the different numerical dissipation mechanisms at work in both schemes. Calculations with other Mach numbers showed analogous results and can be seen as a further validation of the RS-IMEX scheme.

Comparisons of the dissipation rate the compressible kinetic energy as a measure of quality, displayed in Fig. 8, confirm that explicit and RS-IMEX method behave similarly in this setting. Differences are due to the slightly different numerical dissipation added by the Riemann solvers. Concluding, we see that the RS-IMEX splitting is able to reproduce a complex three dimensional physical behavior such as the Taylor-Green vortex.

Focusing on the question of efficiency, the required time for calculations with different discretization methods for several Mach numbers are displayed in Fig. 9. Computational effort increases with decreasing Mach number for the explicit scheme as the time step decreases accordingly. A strong increase of computational effort for the fully implicit scheme is noticeable as the stiffness of the equation system increases. For "high" Mach numbers, more computational time is needed for the RS-IMEX scheme as an additional

partial differential equation has to be approximated. But, only a slight increase in computational effort for decreasing Mach number is observed as the stiffness is hidden in the linear system instead of the non-linear system as for a fully implicit discretization. This constitutes obviously a huge advantage of the RS-IMEX splitting compared to a fully implicit scheme. Whereas the stiffness of the fully implicit scheme is increased in the non-linear system, the Jacobian in Eqn. (9) has to be approximated via the finite difference (10). The approximation of the Jacobian with the finite difference gets worse for an increasing stiffness of the equation system, and therefore, computational time strongly increases for the fully implicit scheme. Using the RS-IMEX splitting the Jacobian can be calculated exactly with Eqn. (11). Hence, an increasing stiffness only slightly increases the computational effort. Consequently, large savings concerning computational costs can be obtained by using the RS-IMEX splitting for very low Mach numbers $\varepsilon < 10^{-3}$ compared to the explicit scheme and $\varepsilon < 10^{-1}$ compared to the implicit scheme.

7 Conclusion and Outlook

The efficient and accurate numerical solution of physical phenomena that belong to the class of singularly perturbed problems is still an area of active research. These problems can be seen as a special case of multi-scale problems, in which large differences in scale with regards to the average state occur in a spatially confined region of the solution. This becomes especially challenging when high accuracy in the limit is sought, i.e. the discretization should obey the underlying asymptotic properties of the equation.

In this work, we have taken steps towards the development of an efficient high order DG scheme for all-speed flows at an engineering scale. Starting from the novel operator splitting technique RS-IMEX for the isentropic Euler equations proposed in [23], we have re-formulated the discrete equations to significantly extend the Mach number range of the scheme without the occurrence of machine accuracy problems and demonstrated its capability to prevent a stall in convergence.

The RS-IMEX splitting has been implemented in an existing high-order DGSEM framework. The incompressible reference solution is solved by an artificial-compressibility type scheme, which couples the velocity and pressure field through a numerical flux function and thereby introduces a hyperbolic equation for the pressure. Numerical results have shown the efficiency of the method also in the context of realistic three-dimensional applications.

Since the RS-IMEX is conceptually independent from the underlying equations, its naive application to other systems is straightforward. However, it is not a priori clear whether this splitting guarantees hyperbolicity of the explicit part. Current research efforts are underway to answer this question and to explore the possibilities of extending the splitting to the full Euler equations. Furthermore, the application of the splitting to multiphase flows is of current interest.

8 Acknowledgment

The authors would like to thank Sebastian Noelle and Nico Krais for the fruitful discussions.

Jonas Zeifang has been supported by the German Research Foundation (DFG) through the International Research Training Group GRK 2160: Droplet Interaction Technologies (DROPIT). The computations with the FLEXI framework have been conducted on the Cray XC40 at the High Performance Computing Center Stuttgart under the *hpcdg* project.

Klaus Kaiser has been partially supported by the German Research Foundation (DFG) through project NO 361/6-1; his study was supported by the Special Research Fund (BOF) of Hasselt University.

9 Appendix

For the purpose of completeness, we list the Runge-Kutta schemes we have used throughout this paper, see Tbl. 1, 2, 3, 4 and 5. The left tableaux of the IMEX-Runge-Kutta schemes denote the Butcher tableaux of the part treated implicitly $\widetilde{(\cdot)}$, the right Butcher tableaux correspond to the explicit part $\widehat{(\cdot)}$.

0	0	0	0	0	0	0	0
γ	0	γ	0	γ	γ	0	0
1	0	$1-\gamma$	γ	1	δ	1-δ	0
	0	$1-\gamma$	γ		δ	1-δ	0

Table 1: 2^{nd} order scheme IMEX-ARS-222 [2] with $\gamma = \frac{2-\sqrt{2}}{2} \approx 0.293$ and $\delta = 1 - \frac{1}{2\gamma} \approx -0.707$.

0	0	0	0	0	0	0	0	0	0	0	0
1/2	0	1/2	0	0	0	1/2	1/2	0	0	0	0
2/3	0	1/6	1/2	0	0	2/3	11/18	1/18	0	0	0
1/2	0	-1/2	1/2	1/2	0	1/2	5/6	-5/6	1/2	0	0
1	0	3/2	-3/2	1/2	1/2	1	1/4	7/4	3/4	-7/4	0
	0	3/2	-3/2	1/2	1/2		1/4	7/4	3/4	-7/4	0

Table 2: 3^{rd} order scheme IMEX-ARS-443 [2]

0	0	0	0	0	0	0	0	0	0	0	0	0	0	0
1/3	-1/6	1/2	0	0	0	0	0	1/3	1/3	0	0	0	0	0
1/3	1/6	-1/3	1/2	0	0	0	0	1/3	1/6	1/6	0	0	0	0
1/2	3/8	-3/8	0	1/2	0	0	0	1/2	1/8	0	3/8	0	0	0
1/2	1/8	0	3/8	-1/2	1/2	0	0	1/2	1/8	0	3/8	0	0	0
1	-1/2	0	3	-3	1	1/2	0	1	1/2	0	-3/2	0	2	0
1	1/6	0	0	0	2/3	-1/2	2/3	1	1/6	0	0	0	2/3	1/6
	1/6	0	0	0	2/3	-1/2	2/3		1/6	0	0	0	2/3	1/6

Table 3: 4^{th} order scheme IMEX-ARK-4A2 [31]

The explicit schemes are given in the $2N$-storage form [11] for the coefficients A_i, B_i and c_i.

References

[1] J. D. Anderson. *Fundamentals of Aerodynamics*. McGraw Hill New York, 2001.

[2] U. M. Ascher, S. Ruuth, and R. Spiteri. Implicit-explicit Runge-Kutta methods for time-dependent partial differential equations. *Applied Numerical Mathematics*, 25:151–167, 1997.

[3] F. Bassi, L. Botti, A. Colombo, D. Di Pietro, and P. Tesini. On the flexibility of agglomeration based physical space discontinuous Galerkin discretizations. *Journal of Computational Physics*, 231:45–65, 2011.

[4] F. Bassi, A. Crivellini, D.A. Di Pietro, and S. Rebay. An artificial compressibility flux for the discontinuous Galerkin solution of the incompressible Navier-Stokes equations. *Journal of Computational Physics*, 218:794–815, 2006.

i	A_i	B_i	c_i
1	0	1/3	0
2	−5/9	15/16	1/3
3	−153/128	8/15	3/4

Table 4: 3^{rd} order low storage explicit Runge-Kutta scheme [44]

i	A_i	B_i	c_i
1	0	$\frac{1432997174477}{9575080441755}$	0
2	$-\frac{567301805773}{1357537059087}$	$\frac{5161836677717}{13612068292357}$	$\frac{1432997174477}{9575080441755}$
3	$-\frac{2404267990393}{2016746695238}$	$\frac{1720146321549}{2090206949498}$	$\frac{2526269341429}{6820363962896}$
4	$-\frac{3550918686646}{2091501179385}$	$\frac{3134564353537}{4481467310338}$	$\frac{2006345519317}{3224310063776}$
5	$-\frac{1275806237668}{842570457699}$	$\frac{2277821191437}{14882151754819}$	$\frac{2802321613138}{2924317926251}$

Table 5: 4^{th} order low storage explicit Runge-Kutta scheme [11]

[5] F. Bassi and S. Rebay. A high-order accurate discontinuous finite-element method for the numerical solution of the compressible Navier-Stokes equations. *Journal of Computational Physics*, 131:267–279, 1997.

[6] A. D. Beck, T. Bolemann, D. Flad, H. Frank, G. J. Gassner, F. Hindenlang, and C.-. Munz. High-order discontinuous Galerkin spectral element methods for transitional and turbulent flow simulations. *International Journal for Numerical Methods in Fluids*, 76(8):522–548, 2014.

[7] P. Birken, G. Gassner, M. Haas, and C.-D. Munz. Preconditioning for modal discontinuous Galerkin methods for unsteady 3D Navier–Stokes equations. *Journal of Computational Physics*, 240:20–35, 2013.

[8] G. Bispen, K.R. Arun, M. Lukáčová-Medvid'ová, and S. Noelle. IMEX large time step finite volume methods for low Froude number shallow water flows. *Communications in Computational Physics*, 16:307–347, 2014.

[9] S. Boscarino. Error analysis of IMEX Runge-Kutta methods derived from differential-algebraic systems. *SIAM Journal on Numerical Analysis*, 45:1600–1621, 2007.

[10] A. Buffa, T. J. R. Hughes, and G. Sangalli. Analysis of a multiscale discontinuous Galerkin method for convection-diffusion problems. *SIAM Journal on Numerical Analysis*, 44(4):1420–1440, 2006.

[11] M.H. Carpenter and C.A. Kennedy. Fourth-order $2N$-storage Runge-Kutta schemes. Technical report, NASA Langley Research Center, 1994.

[12] P. Degond and M. Tang. All speed scheme for the low Mach number limit of the isentropic Euler equation. *Communications in Computational Physics*, 10:1–31, 2011.

[13] D. R. Durran. A physically motivated approach for filtering acoustic waves from the equations governing compressible stratified flow. *Journal of Fluid Mechanics*, 601:365–379, 2008.

[14] S. Fechter and C.-D. Munz. A discontinuous Galerkin-based sharp-interface method to simulate three-dimensional compressible two-phase flow. *International Journal for Numerical Methods in Fluids*, 78(7):413–435, 2015.

[15] F. Filbet and S. Jin. A class of asymptotic-preserving schemes for kinetic equations and related problems with stiff sources. *Journal of Computational Physics*, 229(20):7625–7648, 2010.

[16] D. Flad, A. Beck, and C.-D. Munz. Simulation of underresolved turbulent flows by adaptive filtering using the high order discontinuous Galerkin spectral element method. *Journal of Computational Physics*, 313:1–12, 2016.

[17] F. X. Giraldo and M. Restelli. High-order semi-implicit time-integrators for a triangular discontinuous Galerkin oceanic shallow water model. *International Journal for Numerical Methods in Fluids*, 63(9):1077–1102, 2010.

[18] F. X. Giraldo, M. Restelli, and M. Läuter. Semi-implicit formulations of the Navier-Stokes equations: Application to nonhydrostatic atmospheric modeling. *SIAM Journal on Scientific Computing*, 32(6):3394–3425, 2010.

[19] J. Haack, S. Jin, and J.-G. Liu. An all-speed asymptotic-preserving method for the isentropic Euler and Navier-Stokes equations. *Communications in Computational Physics*, 12:955–980, 2012.

[20] F. Hindenlang, G. Gassner, C. Altmann, A. Beck, M. Staudenmaier, and C.-D. Munz. Explicit discontinuous Galerkin methods for unsteady problems. *Computers and Fluids*, 61:86–93, 2012.

[21] S. Jin. Asymptotic preserving (AP) schemes for multiscale kinetic and hyperbolic equations: A review. *Rivista di Matematica della Universita Parma*, 3:177–216, 2012.

[22] K. Kaiser and J. Schütz. A high-order method for weakly compressible flows. *Communications in Computational Physics (in press)*, 2016.

[23] K. Kaiser, J. Schütz, R. Schöbel, and S. Noelle. A new stable splitting for the isentropic Euler equations. *Journal of Scientific Computing*, 70:1390–1407, 2017.

[24] S. Kawai. Direct numerical simulation of transcritical turbulent boundary layers at supercritical pressures with strong real fluid effects. In *54th AIAA Aerospace Sciences Meeting*. American Institute of Aeronautics and Astronautics, 2016.

[25] S. Kawai, H. Terashima, and H. Negishi. A robust and accurate numerical method for transcritical turbulent flows at supercritical pressure with an arbitrary equation of state. *Journal of Computational Physics*, 300:116–135, 2015.

[26] C. A. Kennedy and M. H. Carpenter. Additive Runge-Kutta schemes for convection-diffusion-reaction equations. *Applied Numerical Mathematics*, 44:139–181, 2003.

[27] S. Klainerman and A. Majda. Singular limits of quasilinear hyperbolic systems with large parameters and the incompressible limit of compressible fluids. *Communications on Pure and Applied Mathematics*, 34:481–524, 1981.

[28] R. Klein. Semi-implicit extension of a Godunov-type scheme based on low Mach number asymptotics I: One-dimensional flow. *Journal of Computational Physics*, 121:213–237, 1995.

[29] D. A. Kopriva. *Implementing Spectral Methods for Partial Differential Equations: Algorithms for Scientists and Engineers*. Springer Publishing Company Incorporated, 1st edition, 2009.

[30] S.-H. Lee. Cancellation problem of preconditioning method at low Mach numbers. *Journal of Computational Physics*, 225(2):1199 – 1210, 2007.

[31] H. Liu and J. Zou. Some new additive Runge–Kutta methods and their applications. *Journal of Computational and Applied Mathematics*, 190(1-2):74–98, 2006.

[32] H. Paillere, C. Viozat, A. Kumbaro, and I. Toumi. Comparison of low Mach number models for natural convection problems. *Heat and mass transfer*, 36(6):567–573, 2000.

[33] W. H. Press, S. A. Teukolsky, W. T. Vetterling, and B. P. Flannery. *Numerical Recipes in Fortran 77: The Art of Scientific Computing. Second Edition*, volume 1. Cambridge University Press, 1996.

[34] N. Qin, D. K. Ludlow, and S. T. Shaw. A matrix-free preconditioned Newton/GMRES method for unsteady Navier-Stokes solutions. *International Journal for Numerical Methods in Fluids*, 33:223–248, 2000.

[35] F. Rieper. On the dissipation mechanism of upwind-schemes in the low Mach number regime: A comparison between Roe and HLL. *Journal of Computational Physics*, 229(2):221–232, 2010.

[36] Y. Saad and M. H. Schultz. GMRES: A generalized minimal residual algorithm for solving non-symmetric linear systems. *SIAM Journal on Scientific and Statistical Computing*, 7:856–869, 1986.

[37] S. Schochet. The mathematical theory of low Mach number flows. *ESAIM: Mathematical Modelling and Numerical Analysis*, 39(03):441–458, 2005.

[38] J. Schütz and K. Kaiser. A new stable splitting for singularly perturbed ODEs. *Applied Numerical Mathematics*, 107:18–33, 2016.

[39] J. Sesterhenn, B. Müller, and H. Thomann. On the cancellation problem in calculating compressible low Mach number flows. *Journal of Computational Physics*, 151(2):597 – 615, 1999.

[40] J. R. Simões-Moreira and J. E. Shepherd. Evaporation waves in superheated dodecane. *Journal of Fluid Mechanics*, 382:63–86, 1999.

[41] M. Sonntag and C.-D. Munz. Efficient parallelization of a shock capturing for discontinuous Galerkin methods using finite volume sub-cells. *Journal of Scientific Computing*, 70(3):1262–1289, 2017.

[42] G. I. Taylor and A. E. Green. Mechanism of the production of small eddies from large ones. *Proceedings of the Royal Society of London. Series A, Mathematical and Physical Sciences*, 158(895):499–521, 1937.

[43] Z. J. Wang, K. Fidkowski, R. Abgrall, F. Bassi, D. Caraeni, A. Cary, H. Deconinck, R. Hartmann, K. Hillewaert, H. T. Huynh, N. Kroll, G. May, P. Persson, B. van Leer, and M. Visbal. High-order CFD methods: Current status and perspective. *International Journal for Numerical Methods in Fluids*, 72:811–845, 2013.

[44] J. H. Williamson. Low-storage Runge-Kutta schemes. *Journal of Computational Physics*, 35:48–56, 1980.

[45] W.-A. Yong. A note on the zero Mach number limit of compressible Euler equations. *Proceedings of the American Mathematical Society*, 133(10):3079–3085, 2005.

[46] H. Zakerzadeh and S. Noelle. A note on the stability of implicit-explicit flux splittings for stiff hyperbolic systems. *IGPM Preprint Nr. 449*, 2016.

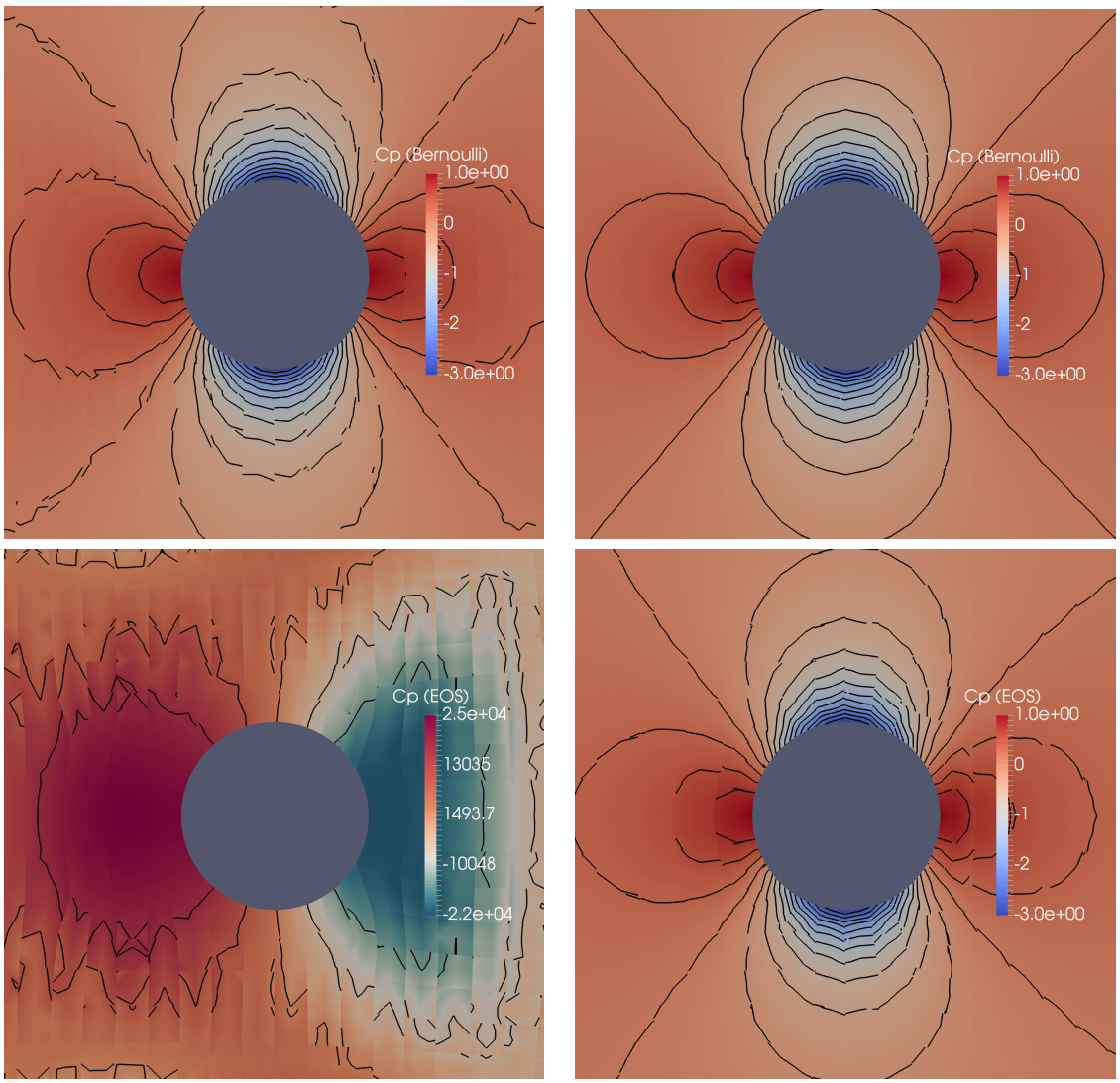

Figure 5: Isolines and colors of pressure coefficient C_p calculated via Bernoulli's hypothesis (upper) and via the equation of state (lower) for 3^{rd} order explicit scheme (left) and RS-IMEX splitting (right) at $\varepsilon = 10^{-5}$.

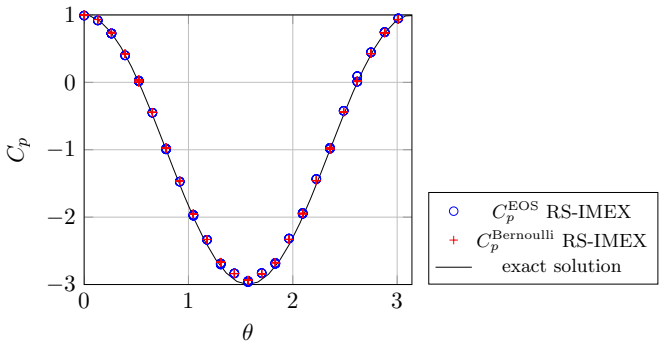

Figure 6: Distribution of C_p^{EOS} and $C_p^{\mathrm{Bernoulli}}$ for 3^{rd} order RS-IMEX splitting at $\varepsilon = 10^{-5}$ calculated with the equation of state or Bernoulli's equation in comparison with potential flow

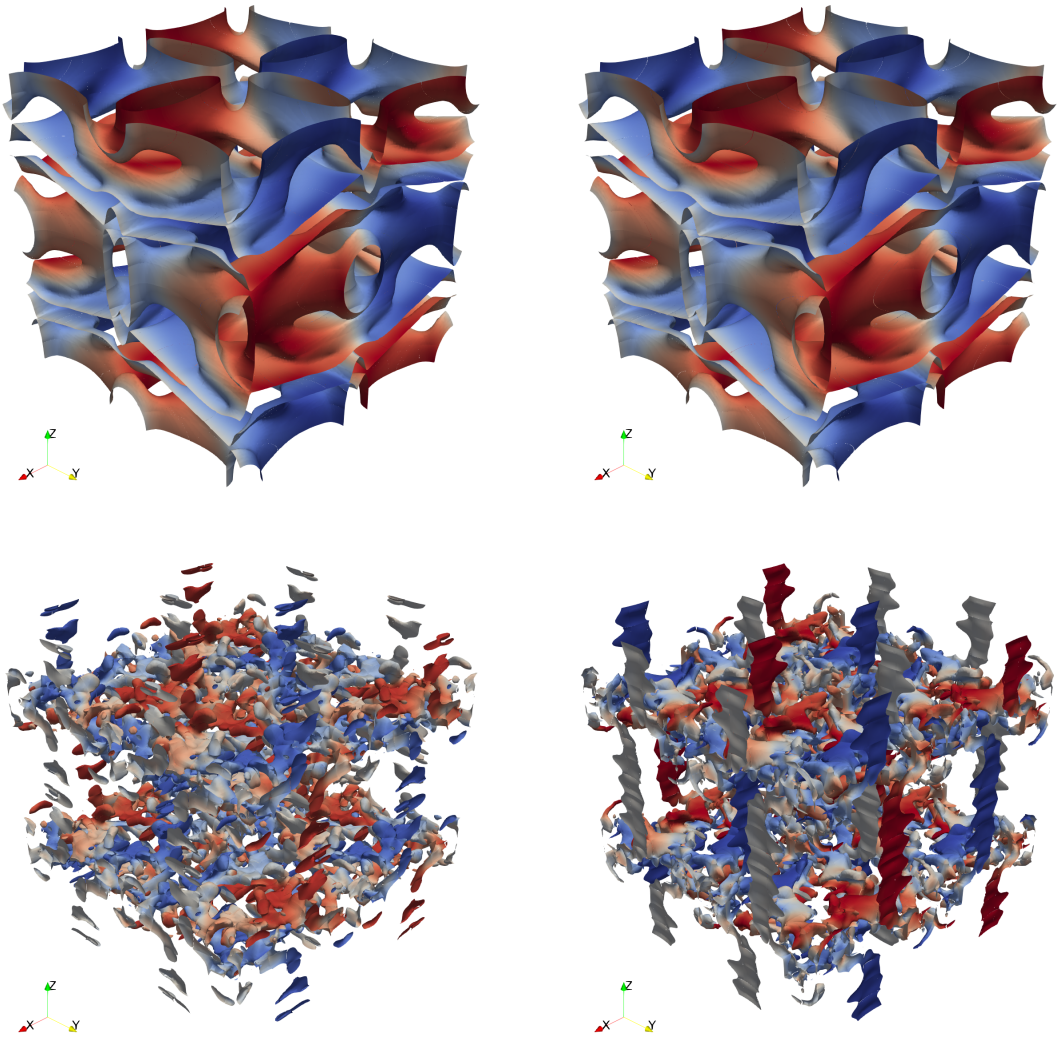

Figure 7: Isosurfaces of velocity magnitude at a physical time of $t = 3s$ (top) and $t = 7s$ (bottom) for explicit (left) and RS-IMEX scheme (right) at $\varepsilon = 10^{-4}$.

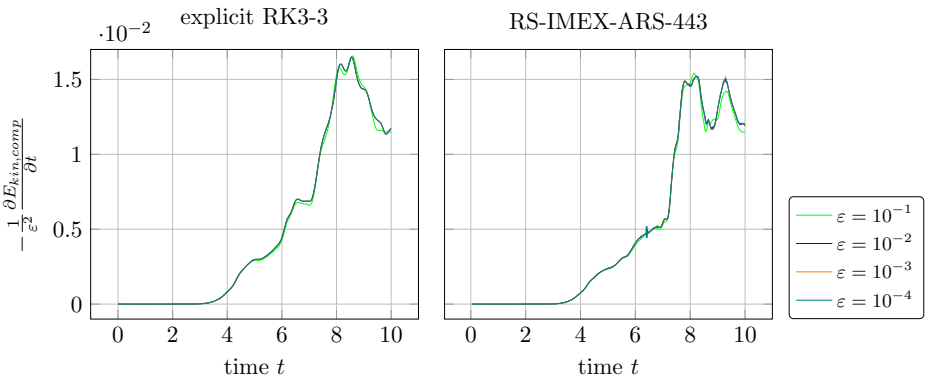

Figure 8: Scaled change rate of compressible kinetic Energy for TGV with explicit scheme (left) and RS-IMEX (right) (both 4^{th} order in space) and Lax-Friedrichs-type Riemann solver.

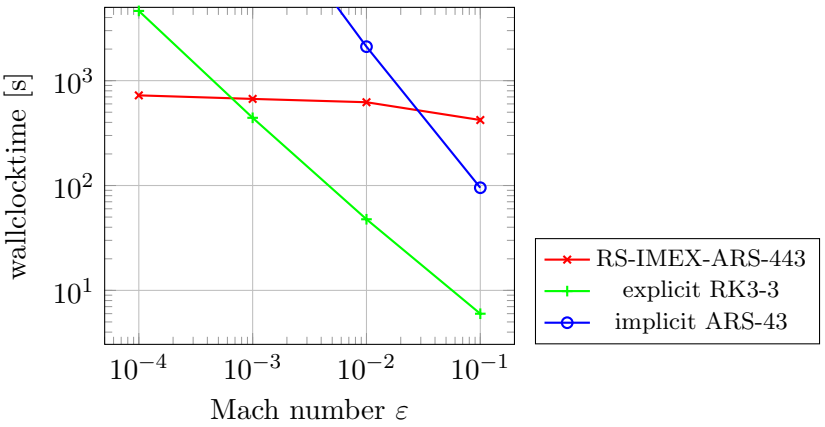

Figure 9: Comparison of computational time with 528 cores of RS-IMEX splitting, explicit and implicit scheme for TGV with 16^3 spatial elements and 4^{th} order in space.

UHasselt Computational Mathematics Preprint Series

2017

UP-17-04 *Jonas Zeifang, Klaus Kaiser, Andrea Beck, Jochen Schütz and Claus-Dieter Munz*, **Efficient high-order discontinuous Galerkin computations of low Mach number flows**, 2017

UP-17-03 *Maikel Bosschaert, Sebastiaan Janssens and Yuri Kuznetsov*, **Switching to nonhyperbolic cycles from codim-2 bifurcations of equilibria in DDEs**, 2017

UP-17-02 *Jochen Schütz, David C. Seal and Alexander Jaust*, **Implicit multiderivative collocation solvers for linear partial differential equations with discontinuous Galerkin spatial discretizations**, 2017

UP-17-01 *Alexander Jaust and Jochen Schütz*, **General linear methods for time-dependent PDEs**, 2017

2016

UP-16-06 *Klaus Kaiser and Jochen Schütz*, **A high-order method for weakly compressible flows**, 2016

UP-16-05 *Stefan Karpinski, Iuliu Sorin Pop, Florin A. Radu*, **A hierarchical scale separation approach for the hybridized discontinuous Galerkin method**, 2016

UP-16-04 *Florin A. Radu, Kundan Kumar, Jan Martin Nordbotten, Iuliu Sorin Pop*, **Analysis of a linearization scheme for an interior penalty discontinuous Galerkin method for two phase flow in porous media with dynamic capillarity effects** , 2016

UP-16-03 *Sergey Alyaev, Eirik Keilegavlen, Jan Martin Nordbotten, Iuliu Sorin Pop*, **Fractal structures in freezing brine**, 2016

UP-16-02 *Klaus Kaiser, Jochen Schütz, Ruth Schöbel and Sebastian Noelle*, **A new stable splitting for the isentropic Euler equations**, 2016

UP-16-01 *Jochen Schütz and Vadym Aizinger*, **A hierarchical scale separation approach for the hybridized discontinuous Galerkin method**, 2016